International Journal of Thermal Sciences 95 (2015) 64–72

Contents lists available at ScienceDirect

International Journal of Thermal Sciences

journal homepage: www.elsevier.com/locate/ijts

Review

Influence of the dynamic boundary conditions on natural convection in an asymmetrically heated channel

B. Brangeon [a, *], P. Joubert [a], A. Bastide [b]

[a] LaSIE, Avenue Michel Crépeau, 17042, La Rochelle Cedex 1, France
[b] PIMENT, 117 Avenue du Général Ailleret, 97430, Le Tampon, France

ARTICLE INFO

Article history:
Received 27 February 2014
Received in revised form
9 April 2015
Accepted 9 April 2015
Available online

Keywords:
Channel-chimney system
Open geometries
Natural ventilation
Boundary conditions
Flow reversal
Theoretical aspects of building performance
modelling and simulation

ABSTRACT

The present paper is concerned with the results of the numerical investigation of unpermanent laminar, natural convection in an asymmetrically heated inclined open channel ($i = 0,45,60$ and 75°) with walls at uniform heat flux ($q_w = 10,50,75$ and 100 W m^{-2}). Two methodological approaches have been adopted to investigate the air flow in these configurations: 2D and 3D description, and four sets of inlet-outlet velocity-pressure boundary conditions have been considered. Significant differences are observed in the flow dynamics between 2D and 3D results. The numerical results are compared with the experimental data and a good agreement is obtained when a local pressure boundary condition is applied at the inlet/outlet sections in the 3D case. A generalized correlation for the average Nusselt number is then obtained from numerical results. This correlation covers a wide range of the modified Rayleigh number and aspect ratio values ($Ra_m\cos(i)$ varying from 1.71×10^4 to 3.60×10^6 and $6.5 < H/b < 12.8$).

1. Introduction

A new generation of computational tools for building and community energy systems will be developed in the near future (Wetter et al. [1], Jin et al. [2]). Their validation will involve comparisons between simulations, analytical solutions and real-scale experiments and inter-model comparisons using existing standards such as ASHRAE Standard. This investigation provides theoretical foundations for buoyant flow analysis in passive systems. Passive systems based on buoyant flows developing in heated vertical or inclined channels are used in many engineering applications such as solar chimneys, photovoltaic cooling systems, or devices for air conditioning and natural ventilation in buildings. Recent papers can be found in the literature for such configurations, as well from an experimental point of view (Chami and Zoughaib [3], Popa et al. [4], Daverat et al. [5]) than for an analytical or numerical point of view (Bassiouny and Korah [6], Suárez et al. [7]), in continuation of numerous previous works during the last decades. Elenbaas [8] pioneered the experimental investigation of natural convection of air within a vertical parallel-plate channels and identified the different types of flows regimes, according to the definition of a modified Rayleigh number. Bar-Cohen and Rohsenow [9] derived a set of correlations for the Nusselt number in an asymmetrically heated channel. Sparrow et al. [10] highlighted on their wall the possibility of a reversal flow at the upper end of a channel heated at a constant temperature on one side. More recently, the domain of existence of reversal flow was deeply experimentally investigated by Dupont et al. [11,12] for a constant flux wall heated channel.

From a numerical point of view, imposition of coherent boundary conditions at the geometrical limits of the computational domain is not obvious because velocity and pressure values are not known *a priori* at the inlet and outlet sections of the channel. Different strategies are then available to improve theoretical aspects of building performance modelling and the open geometries. One is to consider extended spatial domains at the entrance and at the exit of the channel where free stress or non rotational flow conditions can reasonably be applied. Naylor et al. [13] considered as an example a semi-circular virtual extension at the entrance of the channel with a Jeffery [14] or Hamel [15] flow

* Corresponding author.
E-mail address: bbrangeo@gmail.com (B. Brangeon).

http://dx.doi.org/10.1016/j.ijthermalsci.2015.04.006
1290-0729/

Nomenclature

Dimensionless terms

θ	dimensionless temperature
A	surface area
G	dimensionless flow rate
$Nu_{1/2}$	local Nusselt number at mid-height of the channel $\left(\frac{1}{\theta}\right)$
P	dimensionless modified pressure
Pr	Prandtl number (ν/κ)
Ra_H	height-based Rayleigh number $\left(Ra_m\left(\frac{H}{b}\right)^5\right)$
Ra_m	modified Rayleigh number $\left(\frac{g\beta q_w b^4}{\lambda\nu^2}\frac{b}{H}Pr\right)$
Re	Reynolds number $\left(\frac{u\Delta x}{\nu}\right)$
t	dimensionless time
u,w	dimensionless fluid velocity components
x,y,z	dimensionless cartesian coordinates

Greek letters

β	volumetric coefficient of thermal expansion [K^{-1}]
δ	Kronecker symbol
ε	wall emissivity
κ	thermal diffusity [$m^2\ s^{-1}$]
λ	thermal conductivity [$W\ m^{-1}\ K^{-1}$]
ν	kinematic viscosity [$m^2\ s^{-1}$]

Latin letters

$\vec{V}$	velocity vector [$m\ s^{-1}$]
b	characteristic width [m]
g	gravitational acceleration [9.81 $m\ s^{-2}$]
H	channel height [m]
i	inclination angle[°]
l	depth [m]
q_w	heat flux at the wall [$W\ m^{-2}$]
ΔT	temperature difference $(q_w b/\lambda)$ [K]
T_0	inlet temperature [K]
V_b	bulk velocity [$m\ s^{-1}$]
V_{ref}	reference velocity $\left(\frac{\kappa}{H}Ra_H^{1/2}\right)$ [$m\ s^{-1}$]

Subscripts

0	reference
in	channel inlet
BC	boundary condition
GB	global Bernoulli condition
LB	local Bernoulli condition

approximation at the perimeter of this domain. Andreozzi et al. [16] and Campo et al. [17] considered inlet and outlet rectangular extensions at both ends of the channel. The problem of such extensions is that the natural convection flow that develops in the channel is very sensitive to the size of the extensions, and boundary conditions must be rejected far from the inlet/outlet of the channel. Suárez et al. [7] found in that way that the computational domain including the whole channel they consider must be 200 times larger and higher than the channel itself for assuming independence of the flow and heat transfer in the channel from the external surrounding domain.

The problem then turns into the choice of realistic inlet boundary conditions and their numerical implementation (Le Quéré [18], Desrayaud et al. [19]). Hence, it follows that two and three dimensional natural convection in inclined channels with open boundaries has been rarely investigated using inlet-outlet boundary conditions. In order to investigate the influence of the boundary conditions imposed at the ends of a heated vertical or inclined channel on the natural convection flow inside the channel, an in-house numerical code has been developed. The configurations we consider are similar to those experimentally investigated by Webb and Hill [20] and Dupont et al. [11,12]. We defined different sets of pressure–velocity boundary conditions, either for 2D and 3D computations. The experimental data available from the experiments provide relevant information for comparison with the numerical simulations in terms of heat transfer at the heated wall, mass flow rate in the channel, but also for velocity and temperature profiles.

In the first part of the paper, the numerical approach is introduced and different sets of pressure–velocity boundary conditions are discussed in 2D and 3D for a vertical channel. Then numerical results are compared with experimental data, particularly for the existence of a reversal flow for height-based Rayleigh number Ra_H, ranging from 5.89×10^9 to 5.89×10^{10}, for aspect ratio $6.5 < H/b < 12.8$ and tilt angle of the channel $0 < i < 75^\circ$.

Finally, a generalized correlation for the Nusselt number is proposed from the 2D numerical results and compared to existing ones.

2. Problem description

2.1. Geometry

In order to focus on the flow and heat transfer in the channel, we consider in this study a computational domain restricted to the channel geometry. This raises the question of defining a physically coherent set for the boundary conditions at the inlet and outlet of the channel, that enables in particular recirculation of the fluid inside the channel.

First, we consider a two-dimensional open channel asymmetrically heated by a constant parietal heat flux imposed on its left side (see Fig. 1, Dupont et al. [12]). The experimental channel consists in two parallel rectangular plates of dimension $H \times l$ with $H = 0.64$ m made of epoxy resin with copper cover of low emissivity ($\varepsilon = 0.26$) to limit the radiative effects. The front and rear faces are made of glass for measurement facility, and the entrance and exit borders are completed with a convergent, consisting of a quarter-cylinder shape of radius 50 mm. Measurements are achieved with a two-component Dantec Laser Doppler Anemometer (LDA) system for velocity. Wall temperatures were measured by 34 type K, 100 μ m thermocouples. The calibration of the temperature measurement system showed an accuracy of ±0.1 K. In the present investigation, different heat fluxes and channel widths are studied, namely: $q_w = 10$, 50, 75 and 100 $W\ m^{-2}$ and $b = 0.05$, 0.06 and 0.1 m, resulting in aspect ratios (H/b) of the channel equal to 12.8; 10.67 and 6.5 respectively. For three-dimensional numerical investigation the depth $l = 0.304$ m is considered. Thirty two cases were considered, which are summarized in Table 4.

2.2. Governing equations

Computational fluid dynamics (CFD) approach is employed to simulate the airflow and heat transfer in the inclined channel system. The continuity (1a), momentum (1b) and energy (1c) equations for a two or three dimensional laminar flow of an incompressible Newtonian fluid under the Boussinesq

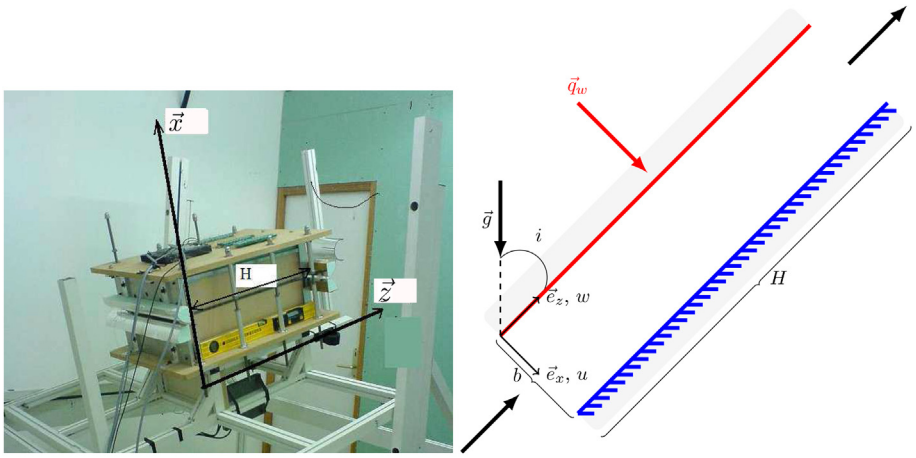

(a) Experimental device Dupont et al. [11, 12] (b) Computational domain

Fig. 1. Asymmetric inclined channel heated at uniform heat flux.

Table 1
Grid sensibility tests.

Case	Grid size	$Ra_H = 5.89 \times 10^9$ $Nu_{1/2}$	$Ra_H = 5.89 \times 10^{10}$ $Nu_{1/2}$
1	64 × 64	5.29	8.08
2	64 × 128	5.30	8.09
3	64 × 512	5.31	8.21
4	128 × 128	5.24	8.21
5	128 × 512	5.24	8.29
6	256 × 1024	5.24	8.29

Table 2
Inlet and outlet pressure boundary conditions.

		Inlet	
		GB	LB
Outlet	0	GB-0	LB-0
	LB	GB-LB	LB-LB

Table 3
Summary of the flow results for $Ra_H = 5.9 \times 10^9$, $H/b = 10.7$ and $i = 0^\circ$.

	$v_b(m\ s^{-1})$	$Nu_{1/2}$
Dupont et al [12]	0.043	–
GB-0	0.047	5.337
GB-LB	0.048	5.343
LB-0	0.040	5.225
LB-LB	0.042	5.239
3D LB-LB	0.042	5.242

approximation are used. The equations in dimensionless form, using H as the reference length, $V_{ref} = \frac{\kappa}{H} Ra_H^{1/2}$ as the reference natural convection velocity, and $\Delta T = q_w b/\lambda$ as temperature difference, are:

$$\vec{\nabla} \cdot \vec{V} = 0 \tag{1a}$$

$$\frac{\partial \vec{V}}{\partial t} + \vec{\nabla} \cdot (\vec{V} \oplus \vec{V}) = -\vec{\nabla} P + \mathrm{Pr} Ra_H^{-1/2} \nabla^2 \vec{V} + Pr\theta \left(\sin(i)\vec{e_x} + \cos(i)\vec{e_z} \right) \tag{1b}$$

$$\frac{\partial \theta}{\partial t} + \vec{\nabla} \cdot (\vec{V}\theta) = Ra_H^{-1/2} \nabla^2 \theta \tag{1c}$$

with $\vec{V} = u\vec{e_x} + v\vec{e_y} + w\vec{e_z}$, Ra_H is the Rayleigh number based on the height of the cavity, and Pr is the Prandtl number. Here β, ν and κ are respectively the coefficient of volumetric expansion, kinematic viscosity, and thermal diffusivity. The thermophysical air properties are all evaluated at the reference temperature $T_0 = 298$ K, so $Pr = 0.71$.

3. Numerical approach

The 2D configuration considered in the present study is presented in Fig. 1(b). The spatial discretization is achieved with a finite-volume method on collocated grids. Time derivatives in the momentum and the energy equations are approximated by a second-order Euler backward differentiation scheme. An implicit

Table 4
Numerical cases with different parameters which have been investigated in the study.

	Ra_H			5.89×10^9	2.95×10^{10}	4.42×10^{10}	5.89×10^{10}
	q_w(W m^{-2}) grid 2D			10 (64 × 512)	50 (128 × 512)	75 (128 × 1024)	100 (256 × 1024)
BC	b(m)	i(°)	H/b	$Ra_m \cos(i)$			
LB-LB	0.05	0	12.8	1.71×10^4	8.57×10^4	1.29×10^5	1.71×10^5
	0.05	45	12.8	1.21×10^4	6.06×10^4	9.09×10^4	1.21×10^5
	0.05	60	12.8	8.57×10^3	4.29×10^4	6.43×10^4	8.57×10^4
	0.05	75	12.8	4.44×10^3	2.22×10^4	3.33×10^4	4.44×10^4
	0.06	0	10.67	4.27×10^4	2.13×10^5	3.20×10^5	4.27×10^5
	0.0985	0	6.5	5.09×10^5	2.54×10^6	3.82×10^6	5.09×10^6
	0.0985	45	6.5	3.60×10^5	1.80×10^6	2.70×10^6	2.54×10^6
	0.0985	60	6.5	2.54×10^5	1.27×10^6	1.91×10^6	3.60×10^6

formulation is employed for the diffusion terms associated with an explicit second-order backward Adams-Bashforth extrapolation for the nonlinear terms. A Pressure Implicit with Splitting of Operators (PISO, Issa [21]) procedure is used for the pressure–velocity coupling. It is to be noted that the maximum local Reynolds number ($Re = u\Delta x/\nu$) obtained was always lower than 10. The dimensionless time step (Δt) varies from 2×10^{-3} to 5×10^{-5} respectively for $Ra_H = 5.89 \times 10^9$ and. $Ra_H = 5.89 \times 10^{10}$

Grid spacing in the z-direction is uniform and the wall–normal points are distributed using a cosine distribution Henkes and Hoogendoorn [22]:

$$x(i) = \frac{b}{2H}\left\{1 - \cos\left(\frac{\pi(i-1)}{N-1}\right)\right\} \quad (2)$$

In a first step, a grid sensibility was performed in the case of an aspect ratio $H/b = 12.8$ for two values of the Rayleigh number. The results in terms of the local Nusselt number at mid-height of the channel are presented in Table 1 for different computational grids. The results show that the local Nusselt number is estimated within a 1% error compared to the best results (case 6) when considering a 64×512 mesh. A 64×512 mesh will then be used for case $Ra_H = 5.89 \times 10^9$ and a $64 \times 32 \times 512$ for 3D case. Convergence criterias of 10^{-7} for the residuals of the velocity components and of 10^{-8} for the residuals of the energy were assumed. For $Ra_H = 5.89 \times 10^{10}$, we used a 256×1024 mesh, because turbulence was expected to be present at this high Rayleigh number. But in fact we must notice that significant level of turbulence was never found, whatever the configuration. This is probably due to the fact that only laminar conditions were considered at the entrance of the channel, which considerably delays the boundary layer transition, as noticed by Fedorov and Viskanta [23]. This constitutes a difference with the experimental conditions of Dupont et al. [12] who reported a turbulence intensity of order 5% at the entrance of the channel.

4. Boundary conditions

The boundary conditions along the walls are the following:

- imposed heat fluxes for the temperature, with $\frac{\partial\theta}{\partial x}(x=0,z) = 1$ on the thermally active wall, and $\frac{\partial\theta}{\partial x}(x=b/H,z) = 0$ on the adiabatic wall;
- non-slip boundary condition for the velocity;
- Neumann boundary condition for the pressure, due to the PISO method;

The imposed conditions at the inlet and the outlet are straightforward for temperature and velocity:

- at the inlet ($z = 0$), $\theta = 0$; $u = 0$ and $\frac{\partial w}{\partial z} = 0$;
- at the outlet ($z = 1$): if $\vec{V}.\vec{n} < 0$, then $\theta = 0$, else $\frac{\partial\theta}{\partial x}(x,1) = 0$; $u = 0$ and $\frac{\partial w}{\partial z} = 0$.

The boundary condition for the pressure at the open ends of the domain requires special attention. Indeed, the induced flow in the channel results from the balance between the buoyancy forces generated by the heat transfer along the wall heated and the pressure losses between the inlet and the outlet of the channel. The mass flow rate is not known *a priori*, and the velocity distribution is no more known neither at the inlet nor at the outlet. Thus, in order to avoid external extended domain, we choose to impose artificial pressure boundary conditions at the inlet of the channel, derived from Bernoulli equation, either in global or local form.

- Global Bernoulli boundary condition (GB):

$$P(x,z) = -\frac{1}{2}\left(\int_0^{b/H} w(x,z)dx\right)^2 = \frac{1}{2A_{in}^2}G^2 \quad (3)$$

where G is the dimensionless mass flow rate and A_{in} is the inlet area.

- Local Bernoulli boundary condition (LB):

$$P(x,z) = -\frac{1}{2}w(x,z)^2 \quad (4)$$

At the outlet, two cases are considered:

- a pure free jet condition ($P = 0$ whatever the direction of the flow), denoted as condition 0
- a mix between a jet condition or a LB condition, depending on the local flow direction: $P = 0$ if $V.n > 0$, LB otherwise, denoted as LB condition.

These considerations result in four sets of boundary conditions, synthesized through notations (GB-0, GB-LB, LB-0 and LB-LB) according to Table 2. For example, the set of boundary condition GB-LB is presented Fig. 2: a GB condition (Eq. (3)) is used at the inlet, and at the outlet, a LB condition (Eq. (4)) is imposed if $V.n < 0$, and a free jet condition if $V.n > 0$.

The choice of these boundary conditions implies that the flow is not disturbed at the channel inlet and that the surrounding environment does not influence the flow within the channel. These conditions of non-interference of the surrounding environment are difficult to obtain experimentally for buoyant induced flow, and this must be kept in mind when comparing with experimental results.

5. Results and discussion

5.1. Boundary conditions comparison for a vertical channel

In this part, we compare the numerical results obtained from 2D and 3D CFD modeling, considering the four preceding sets of boundary conditions, to the experimental data detailed in Dupont et al. [12] for a vertical channel with an aspect ratio $H/b = 10.7$ and a height-based Rayleigh number $Ra_H = 5.9 \times 10^9$ ($q_w = 10\,\mathrm{W\,m^{-2}}$). The profiles of the vertical velocity normalized by the bulk velocity (w/V_b) at heights $z/H = 0.03, 0.27, 0.53, 0.80$ and 0.96 are shown in

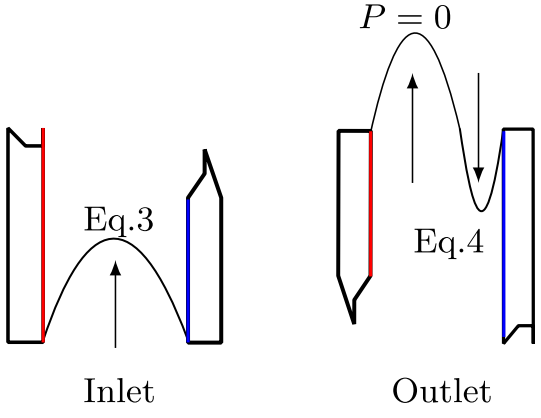

Fig. 2. Example of GB-LB boundary conditions.

Fig. 3(a–e). A 3D computation has been performed for the LB-LB set in order to study the influence of the depth on the flow in the central plane of the channel.

First, we can note as an evidence that, except for the entry section $z/H = 0.03$, the flow reflects the asymmetric thermal boundary conditions along the two opposite vertical walls and exhibits a boundary layer regime along the heated side of the channel. A reversal flow is present in the upper half part of the channel (this will be further investigated in the next section). The so-called chimney effect is not present for this configuration.

In the entry section $z/H = 0.03$, the use of a uniform pressure (GB) induces an asymmetric Poiseuille type velocity profile, while a local pressure boundary condition (LB) provides an essentially flat velocity profile, in better agreement with the experimental profile. But the profil difference rapidly disappears in the first part of the channel (Fig. 3(b)) and the two conditions produce the same shapes of velocity in most part of the channel. First, we can note that there is no significant difference between GB-0 and GB-LB conditions. For LB sets, slight differences can be found in the recirculation region at $z/H = 0.80$ and 0.96, where LB-0 set produces a more pronounced return flow than LB-LB. The main differences are in fact observed between GB-x and LB-x (x = 0 or LB). The global condition at the inlet produce a smoother profile than a local condition, which induces a higher velocity peak value in the boundary layer, and a stronger return flow (Fig. 3(c, d, e)). The local condition overestimates the vertical boundary velocity when compared to the experimental values, but seems to better reproduce the return flow intensity.

We can note in Fig. 3(b–e) a persistent shift in space between the experimental velocity peak and the numerical profiles. One can question about this shift because the experimental profiles exhibit an unrealistic (for this configuration) inflexion point near the heated wall, particularly pronounced for the upper positions. This could be due to an erroneous estimation of the distance to the wall for the LDA measurement volume. An argument for this can be seen in Fig. 3(d and e), where two points are reported at the adiabatic wall, one of them with non null value.

A three-dimensional numerical simulation has been performed with the LB-LB set of boundary condition. Non-slip and adiabatic boundary conditions were applied along the walls in the y-direction. The vertical velocity profiles displayed in Fig. 3(a) show that similar profiles are obtained at the inlet between the 2D and 3D LB-

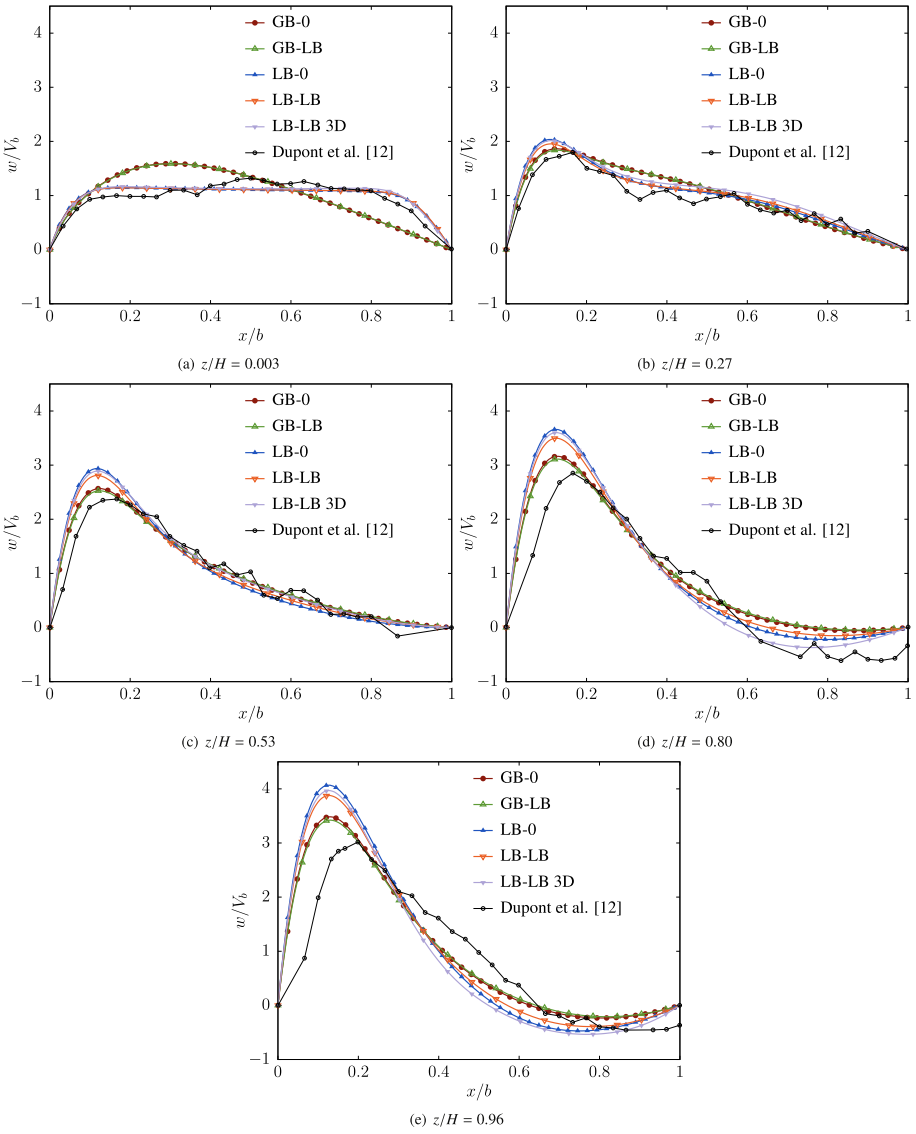

Fig. 3. Vertical velocity profiles w/V_b. Comparison between numerical and experimental results for $Ra_H = 5.9 \times 10^9$, $H/b = 10.7$ and $i = 0^\circ$.

LB cases. However 3D results better represent the reversal flow and slightly improve the comparison with the experimental data through the whole top section of the channel.

A summary of the averaged flow quantities is presented in Table 3 for direct comparison between the different cases we considered. The computed value of the bulk velocity for the LB-LB set of boundary condition goes along with the experimentally observed one. Generally the local pressure condition estimates more precisely the bulk velocity than a global condition, with a difference less than 2% with the experimental value of 0.043 m s^{-1}.

The experimental velocity fields obtained in the channel mid-plane with a Laser Doppler Anemometry technique is represented in Fig. 4(a). The use of this sophisticated technique has been adopted by Dupont et al. [12] due to its low intrusiveness, its spatial resolution and its capacity to differentiate the sign of the velocity. Fig. 4(b–f) show the numerical iso-velocity fields for the four sets of boundary conditions we considered. Comparison of Fig. 4(d) and (e) shows than LB conditions produce a better representation of the flow in the lower section of the channel than GB conditions. The extension of the reversal flow region is also greater for LB than for GB conditions and the intensity of the reversal flow is slightly larger when this local formulation is used (Fig. 4(d) and (e)) versus (Fig. 4(b) and (c)). As already noted in Fig. 3, D case (Fig. 4(f)) improves the prediction of the spatial extension and intensity of the reversal flow.

As a conclusion, LB-LB set of boundary conditions produces the better representation of the experimentally observed reversal flow, and is chosen in the following of this study.

5.2. Parametric study for existence of a reversal flow in a vertical channel

Existence of a reversal flow in a vertical channel has been mentioned inside asymmetric heated channels in laminar conditions by Sparrow et al. [10], Azevedo and Sparrow [24] and Webb and Hill [20]. Dupont et al. [11] studied the existence of reversal flow by varying the aspect ratio (H/b), the heat flux at the wall (q_w), and the inclination angle (i). We studied numerically thirty-two cases reported in Table 4.

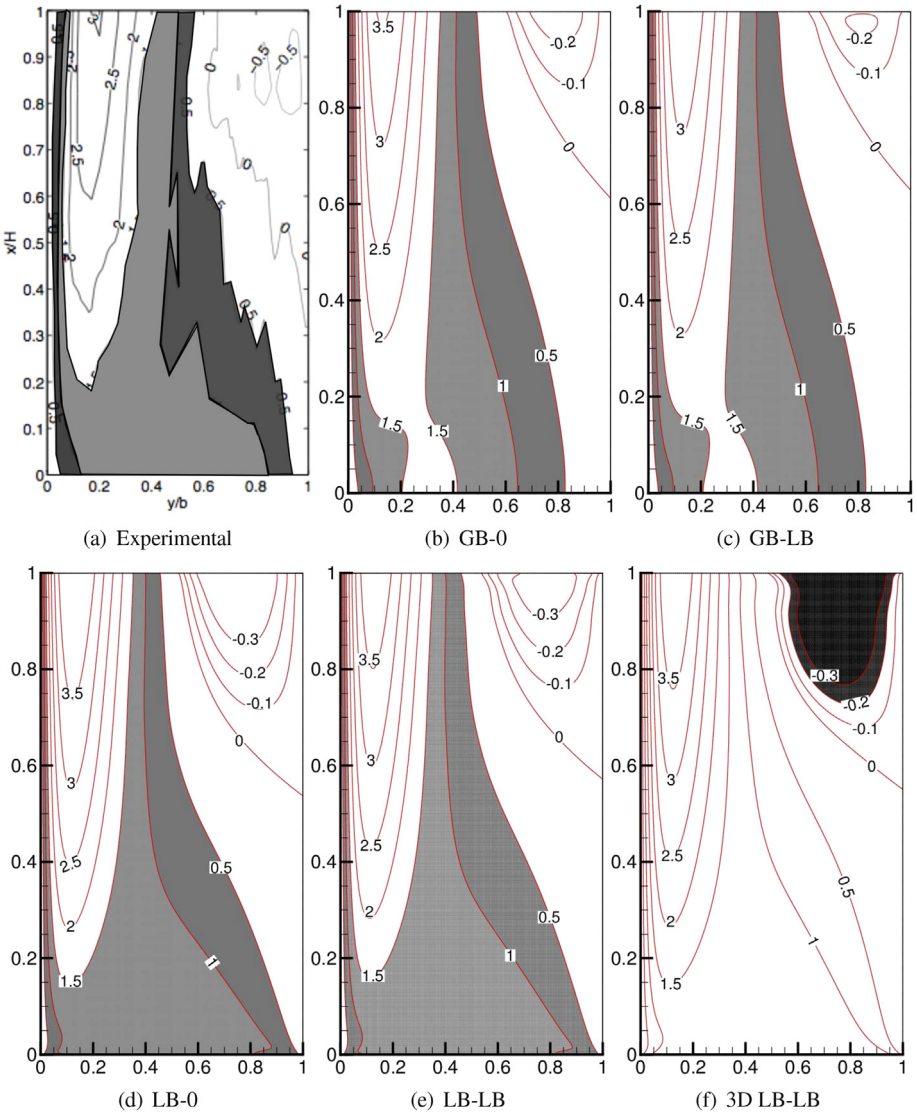

Fig. 4. Iso-contours of w/V_b in the channel for different boundary conditions. $H/b = 10.7$ and $Ra_H = 5.9 \times 10^9$ ($Ra_m \cos(i) = 4.27 \times 10^4$, $q_w = 10\,\mathrm{W\,m^{-2}}$, $i = 0^\circ$). The iso-contours are distributed from −0.3 to 3.5 with a 0.5 step.

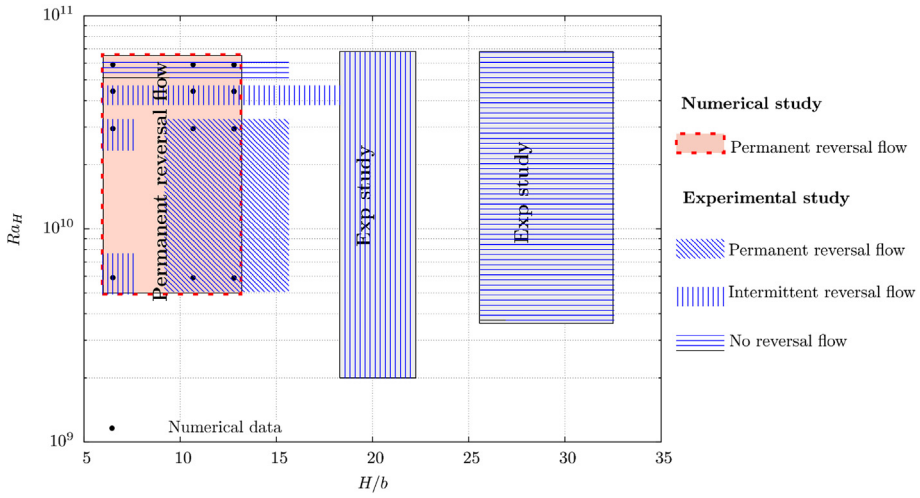

Fig. 5. Existence of reversal flow for $i = 0$. Comparison between numerical and experimental data of Samot et al. [25].

From laser tomography visualizations, Samot et al. [25] explored the conditions of existence of a reversal flow in their channel, and established the following conclusions:

- for values of the aspect ratio H/b between 9.14 and 16 and height-based Rayleigh number (Ra_H) less than 4.46×10^{10}, a permanent reversal flow exists,
- for values of aspect ratio H/b between 18.29 and 25.6 or less than 9; an intermittent reversal flow is observed,
- for values of the aspect ratio H/b greater than 25.6; reversal flow do not exist.

On the contrary, considering our numerical investigation, we observe a permanent reversal flow in all the cases we considered, sometimes with very weak extension, but always present (Fig. 5).

5.3. Heat transfer in inclined channels

5.3.1. Influence of the inclination angle

First, we consider the influence of the inclination angle on the temperature distribution along the heated wall. Two set of results are reported in Fig. 6(a) and Fig. 6(b) at $Ra_H = 5.9 \times 10^9$ and 5.9×10^{10} for $i = 0{,}45$ and 60°. If we compare the temperature evolution along the heated wall (Fig. 6(a) and (b)), we observe the same trends in both cases, with different behaviours between the numerical and the experimental distributions. In this later case, the parietal temperature decreases in the upper section of the channel, as already described by Webb and Hill [20], whilst it continuously grows for the numerical investigation. This difference probably comes from the radiative exchanges between the surrounding walls of the test room and the channel outlet. These exchanges are not taken into account in our numerical results, but various investigations (Li et al. [26], Mittelman et al. [27], Manca and Nardini [28]) report that the flow is extremely sensitive to radiative exchanges between the walls and with the environment. The effect of these radiative exchanges is indeed to increase the temperature distribution on the adiabatic wall and to consequently change the flow structure, as far as preventing the existence of a reversal flow.

5.3.2. Heat transfer correlations

As the heat flux is imposed at the wall, the heat transfer is characterised by the temperature distribution along the heated wall, as seen in the preceding section (5.3.1), and the authors generally also consider the local Nusselt number at mid-height of the cavity ($Nu_{1/2} = 1/\theta$) as a characteristic parameter. Fig. 7 presents the $Nu_{1/2}$ values we obtained compared with the results of Dupont et al. [11] and also with the proposed correlation of Webb and Hill [20] for a vertical channel with adiabatic extensions (Table 5, Eq. (5)). Few differences exist within the results on the mid-height Nusselt numbers, even if the present channel without adiabatic extensions, is not strictly identical to the one of Webb and Hill. Our results tally with the ones obtained by Dupont et al. and match pretty well with Eq. (5), with a relative difference always less than 2%. Dupont et al. [11] proposed a correlation very close to the one of

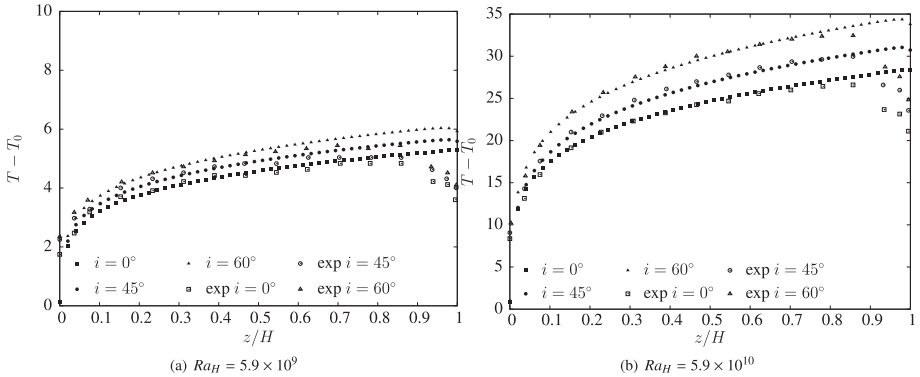

(a) $Ra_H = 5.9 \times 10^9$ (b) $Ra_H = 5.9 \times 10^{10}$

Fig. 6. Wall temperature distribution ($T-T_0$) along the heated wall at $H/b = 6.5$, $T_0 = 298$ K. Comparison between numerical and experimental data of Dupont et al. [11].

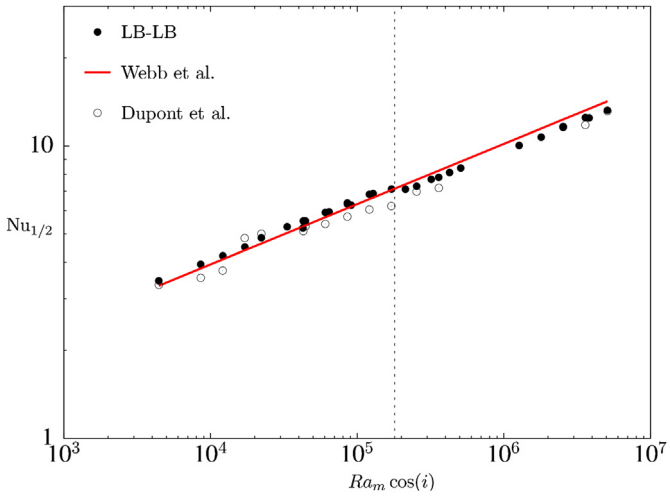

Fig. 7. Local Nusselt number at mid-height of the cavity vs modified Rayleigh number for channel aspect ratios of 6.5, 10.67 and 12.8. Comparison between numerical and experimental data of Webb and Hill [20] and Dupont et al. [11].

Webb and Hill (Table 5, Eqs. (5) and (6)). As can be observed in Fig. 7, a change is present in the $Nu_{1/2}$ evolution at $Ra_m\cos(i) \approx 1.5 \times 10^5$. This value is in good correspondence with the critical modified Rayleigh number observed by Webb and Hill when deriving parameters for the local Nusselt number correlations. So, for better accuracy of the $Nu_{1/2}$ correlation, we propose to divide the whole domain in two sub domains, and to derive correlations for each of theses domains. The first correlation (Eq. (7), Table 5) is valid in the range $4 \times 10^3 < Ra_m\cos(i) \leq 1{,}29 \times 10^5$ ($R^2 = 0.99431$) and the second correlation (Eq. (8), Table 5) is valid in the range $1{,}29 \times 10^5 < Ra_m\cos(i) \leq 5 \times 10^6$ ($R^2 = 0.99262$).

6. Conclusion

We implemented a numerical approach to study the natural convection flows in inclined or vertical open channels. The study was based on an experimental configuration set up by Dupont et al. [11,12] and the comparison with their experimental data was led. The comparisons with the experimental data allow us to highlight the importance of properly chosen boundary conditions for open geometries. We observe than local pressure boundary conditions at the inlet/outlet sections (LB-LB) improve the results when compared to global conditions (GB). Three-dimensional effects were also studied, and show negligible effects for the main upward flow but improve the prediction of the reversal flow. The comparison reveals a correct qualitative accord, but however, differences exist for the domain of existence of a return flow in the upper part of the channel, which brings us to consider the influence of surface radiation on the flow. In fact, surface radiative exchanges influence the flow, particularly near the inlet and outlet sections, and must be considered in this type of configuration. The first results presented in this study will thus be completed in the near future by integrating surface radiation. Lastly, two correlations are also proposed for the local Nusselt number at mid-height of the cavity.

Table 5
Nusselt correlations.

References	Correlations	
Webb and Hill [20]		
	$Nu_{1/2} = 0.58(Ra_m\cos(i))^{0.206}$	(5)
Dupont et al [11]		
	$Nu_{1/2} = 0.59(Ra_m\cos(i))^{0.206}$	(6)
Present		
	$Nu_{1/2} = 0.62(Ra_m\cos(i))^{0.204}$	(7)
	$Nu_{1/2} = 0.72(Ra_m\cos(i))^{0.187}$	(8)

Acknowledgements

This work has been supported by French Research National Agency (ANR) through "Habitat intelligent et solaire photovoltaïque" program (project 4C n° ANR-08-HABISOL-019). The authors thank the reviewers for their remarks which allow to greatly improve the paper.

References

[1] M. Wetter, C. van Treeck, J. Hensen, New generation computational tools for building and community energy systems, IEA EBC Annex. 60 (2013).
[2] M. Jin, W. Liu, Q. Chen, Simulating buoyancy-driven airflow in buildings by coarse-grid fast fluid dynamics, Build. Environ. 85 (2015) 144–152.
[3] N. Chami, A. Zoughaib, Modeling natural convection in a pitched thermosyphon system in building roofs and experimental validation using particle image velocimetry, Energy Build. 42 (2010) 1267–1274.
[4] C. Popa, D. Ospir, S. Fohanno, C. Chereches, Numerical simulation of dynamical aspects of natural convection flow in a double-skin façade, Energy Build. 50 (2012) 229–233.
[5] C. Daverat, H. Pabiou, C. Ménézo, H. Bouia, S. Xin, Experimental investigation of turbulent natural convection in a vertical water channel with symmetric heating: flow and heat transfer, Exp. Therm. Fluid Sci. 44 (2013) 182–193.
[6] R. Bassiouny, N. Korah, Effect of solar chimney inclination angle on space flow pattern and ventilation rate, Energy Build. 41 (2009) 190–196.
[7] C. Suárez, P. Joubert, J. Molina, F. Sánchez, Heat transfer and mass flow correlations for ventilated facades, Energy Build. 43 (2011) 3696–3703.
[8] W. Elenbaas, Heat dissipation of parallel plates by free convection, Physica 11 (1942) 1–23.
[9] A. Bar-Cohen, W. Rohsenow, Thermally optimum spacing of vertical, natural convection cooled, parallel plates, J. Heat Transf. 106 (1984) 116–123.
[10] E. Sparrow, G. Chrysler, L. Azevedo, Observed flow reversals and measured-predicted nusselt numbers for natural convection in a one-sided heated vertical channel, J. Heat Transf. 106 (1984) 325–332.
[11] F. Dupont, T. Soubdhans, R. Blonbou, J. Tuhault, F. Penot, Etude expérimentale de la convection naturelle en canal vertical chauffé à flux constant : Influence de l'angle d'inclinaison, in: Congrés Français de Thermique, 2007.
[12] F. Dupont, F. Ternat, S. Samot, R. Blonbou, Two-dimension experimental study of the reverse flow in a free convection channel with active walls differentially heated, Exp. Therm. Fluid Sci. 47 (2013) 150–157.
[13] D. Naylor, J. Floryan, J. Tarasuk, Numerical study of developing free convection between isothermal vertical plates, J. Heat Transf. 113 (1991) 620–626.
[14] G. Jeffery, The two-dimensional steady motion of a viscous fluid, Philos. Mag. 29 (1915) 455–465.
[15] G. Hamel, Spiralfömrige bewegungen zäher flüssigheiten, Jahresber. Dtsch. Mathematiker-Vereinigung 25 (1916) 34–60.
[16] A. Andreozzi, B. Buonomo, O. Manca, Numerical investigation on natural convection in asymmetric channel-chimney systems, in: WIT Transactions on Modelling and Simulation, vol. 46, 2007, pp. 389–398.
[17] A. Campo, O. Manca, B. Morrone, Inflow and outflow effects on natural convection in partially heated vertical parallel plate channels, in: American Society of Mechanical Engineers, vol. 351, Heat Transfer Division, (Publication) HTD, 1997, pp. 325–335.
[18] P. Le Quéré, On the computation of some external or partially enclosed natural convection flows, in: The 19th International Symposium on Transport Phenomena, Reykjavik, Iceland, 2008, pp. 1–8.
[19] G. Desrayaud, E. Chénier, A. Joulin, A. Bastide, B. Brangeon, J. Caltagirone, Y. Cherif, R. Eymard, C. Garnier, S. Giroux-Julien, Y. Harnane, P. Joubert, N. Laaroussi, S. Lassue, P. Le Quéré, R. Li, D. Saury, A. Sergent, S. Xin, A. Zoubir, Benchmark solutions for natural convection flows in vertical channels submitted to different open boundary conditions, Int. J. Therm. Sci. 72 (2013) 18–33.
[20] B. Webb, D. Hill, High Rayleigh number laminar natural convection in an asymmetrically heated vertical channel, J. Heat Transf. 111 (1989) 649–656.
[21] R. Issa, Solution of the implicitly discretised fluid flow equations by operator-splitting, J. Comput. Phys. 62 (1986) 40–65.

[22] R. Henkes, C. Hoogendoorn, Comparison exercise for computations of turbulent natural convection in enclosures, numerical heat transfer, Part B, Fundam. 28 (1995) 59–78.
[23] A. Fedorov, R. Viskanta, Turbulent natural convection heat transfer in an asymmetrically heated, vertical parallel-plate channel, Int. J. Heat Mass Transf. 40 (1997) 3849–3860.
[24] L. Azevedo, E. Sparrow, Natural convection in open-ended inclined channels, J. Heat Transf. 107 (1985) 893–901.
[25] S. Samot, F. Dupont, F. Penot, Mesure de température dans un écoulement renversé à la sortie d'un thermosiphon vertical chauffé à flux constant, in: Congrés Français de Thermique, Touquet, 2010.
[26] R. Li, M. Bousetta, E. Chénier, G. Lauriat, Effect of surface radiation on natural convective flows and onset of flow reversal in asymmetrically heated vertical channels, Int. J. Therm. Sci. 65 (2013) 9–27.
[27] G. Mittelman, A. Alshare, J. Davidson, A model and heat transfer correlation for rooftop integrated photovoltaics with a passive air cooling channel, Sol. Energy 83 (2009) 1150–1160.
[28] O. Manca, S. Nardini, Thermal design of uniformly heated inclined channels in natural convection with and without radiative effects, Heat. Transf. Eng. 22 (2001) 13–28.